NIH Public Access
Author Manuscript
Med Image Comput Comput Assist Interv. Author manuscript; available in PMC 2014 July 18.

Published in final edited form as:
Med Image Comput Comput Assist Interv. 2013 ; 16(0 3): 510–517.

Diffusion Propagator Estimation from Sparse Measurements in a Tractography Framework

Yogesh Rathi[1], **Borjan Gagoski**[1], **Kawin Setsompop**[1], **Oleg Michailovich**[2], **P. Ellen Grant**[1], and **Carl-Fredrik Westin**[1]

[1]Harvard Medical School, Boston

[2]Department of Electrical Engg., University of Waterloo, Canada

Abstract

Estimation of the diffusion propagator from a sparse set of diffusion MRI (dMRI) measurements is a field of active research. Sparse reconstruction methods propose to reduce scan time and are particularly suitable for scanning un-coperative patients. Recent work on reconstructing the diffusion signal from very few measurements using compressed sensing based techniques has focussed on propagator (or signal) estimation at each voxel independently. However, the goal of many neuroscience studies is to use tractography to study the pathology in white matter fiber tracts. Thus, in this work, we propose a joint framework for robust estimation of the diffusion propagator from *sparse measurements* while simultaneously tracing the white matter tracts. We propose to use a novel multi-tensor model of diffusion which incorporates the bi-exponential radial decay of the signal. Our preliminary results on in-vivo data show that the proposed method produces consistent and reliable fiber tracts from very few gradient directions while simultaneously estimating the bi-exponential decay of the diffusion propagator.

1 Introduction

To obtain accurate information about the neural architecture, diffusion spectrum imaging (DSI) was proposed by [1]. However, this technique requires many measurements, making it impractical to use in clinical settings. Consequently, other imaging and analysis schemes, which use fewer measurements have been proposed in [2–6]. These techniques acquire important information about the neural tissue, which is missed by HARDI methods, yet, only a few of these are used in clinical studies. Traditional methods that compute the entire propagator incorporating the non-monoexponential decay of the signal, require many measurements at high b-values (greater than 3000 s/mm^2) [7, 8], making the scan time too long for un-cooperative patients. Thus, reducing the number of measurements is an important step towards making these techniques clinically viable.

Several methods have used the concept of compressed sensing to dramatically reduce the number of measurements [5, 9–12]. However, all of these methods estimate the fiber orientation distribution function (fODF) or the ensemble average propagator (EAP) at each voxel independently. Tractography is done as a post-processing step, making it susceptible to errors in estimation of the principal diffusion direction. On the other hand, most neuroscience studies require tractography to analyze white matter fiber paths. Thus, we propose a joint framework for tractography and EAP estimation using a causal filter - the

NIH-PA Author Manuscript
NIH-PA Author Manuscript
NIH-PA Author Manuscript

NIH-PA Author Manuscript

NIH-PA Author Manuscript

NIH-PA Author Manuscript

unscented Kalman filter (UKF), allowing for incorporating the correlation in water diffusion along the fiber tracts. With experiments on in-vivo data, we show that the proposed framework is rather robust to the number of measurements required, giving very similar results for sparse as well as dense set of measurements spread over two b-value shells (1000 and 4000 s/mm^2). Thus, we propose a model based framework which is an alternative to the compressed sensing based techniques in terms of the number of measurements required to accurately represent the bi-exponential decay of the diffusion signal.

2 Our Contribution

The proposed work has several novel contributions and extends the work of [13] in a significant way; *(i)* The method in [13] uses a multi-tensor model with the assumption of a mono-exponential signal decay, making it inaccurate for use with high b-values. Note that, several studies have established the bi-exponential decay of diffusion signal at high b-values [8]. Thus, we propose a novel multi-tensor bi-exponential model of diffusion to represent the signal in the entire q-domain, which also has an analytical form for computing the diffusion propagator (EAP). Further, this representation is not limited to the spherical sampling scheme as required by methods based on spherical functions. *(ii)* The proposed UKF based method is robust enough for estimation of the EAP with very few measurements, thus allowing for reducing the number of measurements required. *(iii)* Most sparsity based methods report error in estimation of the EAP at an individual voxel level, making it difficult to asses its effect on estimation of long and short range fiber tracts. To the best of our knowledge, for the first time, we compare the effect of using different number of measurements on tracing several different fiber bundles on a very high b-value data set. We also report error in estimation of return-to-origin probability (RTOP), a measure derived from EAP, for each fiber bundle. *(iv)* Further, we propose a novel probabilistic overlap metric to compute fiber bundle overlap, which is less sensitive to noise.

3 Methods

The diffusion signal $S(\mathbf{q}) : \mathbb{R}^3 \rightarrow \mathbb{R}^+$ is a real-valued function, which determines the value of S at location $\mathbf{q}$ in q-space. Alternatively, S can also be written as a function of b and a unit vector $\mathbf{u}$, such that $S(b, \mathbf{u}) : \mathbb{R} \times \mathbb{S}^2 \rightarrow \mathbb{R}^+$, where $b = (2\pi q)^2 (\Delta - \frac{\delta}{3}) = (2\pi q)^2 \tau$ with δ being the duration of the gradient pulse, Δ is the time between the gradients and $q = \| \mathbf{q} \|$.

Signal Model

At low b-values, the signal decay as a function of b can be approximated by a Gaussian, however at higher b-values, the signal decay is markedly bi-exponential in nature [7, 14]. Signal from high b-values can provide subtle information about the tissue, such as, fast and slow diffusion fractions, which cannot be obtained by assuming a mono-exponential decay. Further, as shown in [15], high b-value data is more sensitive to minor changes in the underlying tissue. Consequently, we propose a novel multi-tensor bi-exponential model to represent the diffusion signal in the entire q-space as follows:

NIH-PA Author Manuscript

NIH-PA Author Manuscript

NIH-PA Author Manuscript

$$S(b,\mathbf{u}) = \frac{1}{n}\sum_{i=1}^{n} w\exp(-b\mathbf{u}^T D_i\mathbf{u}) + (1-w)\exp(-b\mathbf{u}^T \overline{D}_i\mathbf{u}), \quad (1)$$

where w is the weight fraction of the fast diffusing component, $D_i = \lambda_1\mathbf{m}\mathbf{m}^T + \lambda_2(\mathbf{p}\mathbf{p}^T + \mathbf{v}\mathbf{v}^T)$ and $\bar{D}_i = \lambda_3\mathbf{m}\mathbf{m}^T + \lambda_4(\mathbf{p}\mathbf{p}^T + \mathbf{v}\mathbf{v}^T)$ are the diffusion tensors, where we have assumed a cylindrical shape for the diffusion tensor as in [13]. The corresponding diffusion propagator (EAP) has the following analytical form:

$$P(\mathbf{r}) = \frac{1}{n}\sum_{i=1}^{n} \sqrt{\frac{w}{(4\pi\tau)^3|D_i|}}\exp\left(\frac{\mathbf{r}^T D_i^{-1}\mathbf{r}}{4\tau}\right) + \sqrt{\frac{(1-w)}{(4\pi\tau)^3|\overline{D}_i|}}\exp\left(\frac{\mathbf{r}^T \overline{D}_i^{-1}\mathbf{r}}{4\tau}\right). \quad (2)$$

Several analytical formulae can be derived from this expression, for example, the return-to-origin probability (RTOP) $P(0)$, is simply given by:

$$P(0) = \frac{1}{n}\sum_{i=1}^{n} \sqrt{\frac{w}{(4\pi\tau)^3|D_i|}} + \sqrt{\frac{(1-w)}{(4\pi\tau)^3|\overline{D}_i|}}. \quad (3)$$

Modeling Assumptions

From reported experimental data [14] and some *apriori* knowledge about the human anatomy, we make certain assumptions about the model in (1), which allows us to reduce the number of unknowns while allowing for a robust estimation of the parameters. First, we assume that the fast and slow diffusing tensors D_i and $\bar{D}_i$ have the same orientation but different shapes, i.e. different eigenvalues. This is a reasonable assumption, since the fast and slow diffusing components essentially sample the same biological tissue, albeit at different diffusion times (given by the low and high b-value data). Thus, they have the same orientation and differ only in the "amount" of diffusion in different directions, which can be easily represented using the two eigenvalues λ_3, λ_4 of $\bar{D}_i$. Similar to the work in [13, 16], in this preliminary work, we restrict our experiments to the case where $n = 2$ assuming at-most two fiber crossings. The proposed framework is however general enough to be used for three fiber crossings as well. This could be done by adaptively adding a third component if one of the two tensor components becomes planar, indicating a three-fiber crossing. Experiments done in [14] have shown that throughout the brain, the fraction of fast diffusing component is around 0.7, while the slow fraction is 0.3. We thus fix $w = 0.7$ in our work. This, however does not preclude us from modeling other diffusion fractions as can be seen by adjusting the eigenvalues: $\exp(-b\mathbf{u}^T D\mathbf{u}) = \exp(-b\mathbf{u}^T (D_{iso} + D_2)\mathbf{u}) = \alpha\exp(-b\mathbf{u}^T D_2\mathbf{u})$, where we have decomposed a diffusion tensor D into a sum of isotropic tensor D_{iso} and an anisotropic part D_2 leading to $\alpha = \exp(-bD_{iso})$. Thus, changing the eigenvalues is equivalent to changing the volume fraction of the diffusion tensor. This also proves that bi-exponential models cannot have a unique solution. In our case, the UKF acts as a regularizer resulting in smooth parameter estimation.

Thus, the number of unknowns per tensor compartment is 7 (3 for the eigenvector $\mathbf{m}$, 2 eigenvalues of tensor D_i and 2 eigenvalues of tensor $\bar{D}_i$). For a two-fiber model, the total

NIH-PA Author Manuscript

NIH-PA Author Manuscript

NIH-PA Author Manuscript

number of unknowns is 14. Note that, the proposed model is different from that of [7], where the restricted compartment is modeled in terms of the axonal diameter. On the other hand, the model of [14] is a general model with a separate bi-exponential fit done for each gradient direction. This model does not account for consistency in the spherical domain, making the estimation quite susceptible to noise (which is significant at high b-values). The NODDI model [17] utilizes Watson functions for representing the intra-cellular components and a customized acquisition sequence for optimal performance.

Unscented Kalman Filter

We use the unscented Kalman filter (UKF), as described in [13], for robust estimation of the parameters in (1). The UKF framework has the advantage of estimating the model parameters and performing tractography simultaneously, resulting in an inherent regularization of the model parameters and the tracts themselves. To use this state-space filter for estimating the model parameters, we define the following four filter components: *(1)* The system state (**x**): the model parameters, *(2)* The state transition function (*f*): how the model changes as we trace the fiber, *(3)* The observation function (*h*): how the signal appears given a particular model state, *(4)* The measurement (**y**): the actual signal obtained from the scanner.

The state **x** of the system consists of the parameters of the model given by: $\mathbf{x} = [\mathbf{m}_1\ \lambda_{11}\ \lambda_{12}\ \lambda_{13}\ \lambda_{14}\ \mathbf{m}_2\ \lambda_{21}\ \lambda_{22}\ \lambda_{23}\ \lambda_{24}]$. As in [13], we assume the state transition function to be an identity matrix, since the diffusion signal does not change much when stepping from one location to the next within a voxel (we take very small step size). The observation function $h(\mathbf{x})$ is given by equation (1), which "predicts" the signal based on the model parameters **x**. Finally, **y** is the signal measured by the scanner (we perform interpolation as in [13] to obtain the signal at sub-voxel locations). The UKF allows for recursive estimation of the parameters **x** and the confidence in the estimation of **x** via a covariance matrix *P*. This is extremely important, since model parameters (and the corresponding tracts) estimated with low confidence can essentially be discarded.

To initialize the model parameters **x**, we first estimate a single tensor using the low b-value data to obtain the principal diffusion direction **m**. Next, the UKF is run for several iterations (typically 20) at the same location to obtain a reasonable estimate of the initial set of parameters for the bi-exponential model (1). Next, we start the tractography process, by alternately estimating the parameters **x** and taking a small step in the direction of the principal diffusion direction, until a suitable termination criteria is reached.

4 Experiments

We performed several experiments on in-vivo human data to demonstrate the efficacy of the proposed method in computing the EAP and tracing the fiber tracts. Our data set involved 4 different acquisitions of one subject done during the same scanning session. The scans were acquired with $N = \{32, 40, 60, 120\}$ gradient directions at the following b-value shells: $b = \{1000, 4000\} s/mm^2$ and spatial resolution of $2.5 mm^3$. We acquired different sparsely sampled scans to avoid interpolating the densely sampled data and sub-sampling it, which could potentially introduce errors and change the actual SNR (due to smoothing in the

NIH-PA Author Manuscript

NIH-PA Author Manuscript

NIH-PA Author Manuscript

interpolation process). In addition a T1 and T2-weighted images with $1mm^3$ resolution were also acquired with a total scan time of 61 minutes. All diffusion images (of all scans) were spatially normalized and corrected for motion and eddy current distortions using FLIRT [18]. T1-image parcellation was performed with CMTK (www.nitrc.org/projects/cmtk) using the SRI24 atlas [19] and it was subsequently registered to the diffusion space.

We performed whole brain tractography on each of the four data sets, using the proposed method, by seeding 10 times (random) per voxel. Several fiber bundles connecting two regions in the SRI24 atlas were extracted for subsequent analysis. Figure 1 shows tracts connecting the precentral areas in the left and right hemisphere. On the left, we show the tracts obtained with dense sampling of 120 measurements (60 gradient directions per shell) and color coded with the return-to-origin probability (RTOP). As expected, RTOP is low in gray matter (yellow-red) and high white matter (green-blue). Figure 1 (right) also shows the precentral fiber bundles obtained using all the four sampling schemes; red(N = 120), green(N = 60), blue(N = 40) and white(N = 32). Note that, all the other fiber bundles overlap significantly with the one obtained using dense sampling (red). In Figure 2, we show two views of a part of the cortico-spinal tract (CST) obtained by selecting fibers that pass through the internal capsule. For the sake of clarity, we show results for N = 120 (red) and N = 32 (white).

Next, we provide some quantitative results on how well the proposed method traces various fiber bundles (from different scans) relative to the dense sampling method (gold standard) with N = 120. To quantify the overlap between two fiber bundles, we propose to use the Bhattacharyya metric B on probability distributions [20]. We compute probability distribution for each of the spatial co-ordinates (x, y, z) of a fiber bundle (denote the probability distribution function (pdf) on the x-coordinate of the gold standard as $p_g(x)$).

Then, the Bhattacharyya metric B_x is given by: $B_x = \int \sqrt{p_g(x)p(x)}dx$, where $p(x)$ is the pdf of a fiber bundle to be compared. To compute the distance between two fiber bundles, we simply take an equally-weighted combination in each co-ordinate:

$$B = \frac{1}{3}\left(\int \sqrt{p_g(x)p(x)}\,dx + \int \sqrt{p_g(y)p(y)}\,dy + \int \sqrt{p_g(z)p(z)}\,dz\right).$$

This metric has several advantages: 1). The values of B are bounded between 0 and 1. Thus, B will be 1 for a perfect match between two fiber bundles and 0 for no overlap at all. 2). Since the probability distributions are smooth, the metric accounts for minor deviations in tracts due to noise (as opposed to discretizing the fibers to obtain a label map for computing the dice coefficient).

We selected 66 different cortical regions from the SRI24 atlas and computed B for each of the fiber bundles that connected these regions. Fiber bundles obtained using N = 120 measurements were considered as the “gold standard” and distance (B) between fiber bundles obtained with sparser set of measurements were computed. Figure 3 shows the connectivity network for the three different acquisitions color coded with the distance B between the fiber bundles. Note that, B varies between 0.8 and 0.9 for all the acquisitions

NIH-PA Author Manuscript

NIH-PA Author Manuscript

NIH-PA Author Manuscript

indicating a good overlap of the traced fibers. Further, as expected, the acquisition with N = 120 is closest to the gold standard, while the one with N = 32 has only a few fiber bundles with overlap close to 0.8.

We performed a similar analysis on the network, by computing the normalized mean error E in estimation of RTOP for each of the fiber bundles ($E=\frac{|m_g-m|}{m_g}$, where m_g and m is the mean RTOP for the gold standard and the other fiber bundle respectively). Figure 4 shows result for all the three acquisitions (with the dense one being the gold standard). In general, the percentage error in estimation of RTOP is small (around 2–3%), which is close to the variability between two different scans of the same subject. However, there are a few fiber bundles for which the percentage is around 10%, specially for the N = 32 acquisition data.

5 Conclusion and limitations

In this work, we proposed a novel bi-exponential multi-tensor tractography framework for consistent estimation of the diffusion propagator and fiber tracts. We investigated our technique on four different data sets from the same subject but with different number of gradient directions. Our quantitative results showed that the tracts traced with sparser set of samples (N = 32, 40, 60) showed good overlap with those traced using dense sampling of N = 120. Further, the estimated diffusion measure of return-to-origin probability (RTOP) for sparser data sets was quite consistent with that obtained from the dense one. We should however note that, this work is quite preliminary in nature and essentially a proof-of-concept. Our future work entails comprehensive comparison on several subjects as well as quantifying error in different diffusion measures.

Acknowledgments

This work has been supported by NIH grants: R01MH 097979, R01MH074794, P41RR013218, P41EB015902 and VR grant 2012–3682.

References

1. Wedeen V, Hagmann P, Tseng W, Reese T, Weisskoff R. Mapping complex tissue architecture with diffusion spectrum magnetic resonance imaging. Magnetic Resonance in Medicine. 2005; 54(6): 1377–1386. [PubMed: 16247738]
2. Wu Y, Alexander A. Hybrid diffusion imaging. NeuroImage. 2007; 36(3):617–629. [PubMed: 17481920]
3. Jensen J, Helpern J, Ramani A, Lu H, Kaczynski K. Diffusional kurtosis imaging: The quantification of non-gaussian water diffusion by means of magnetic resonance imaging. Magnetic Resonance in Medicine. 2005; 53(6):1432–1440. [PubMed: 15906300]
4. Assemlal HE, Tschumperlé D, Brun L, Siddiqi K. Recent advances in diffusion MRI modeling: Angular and radial reconstruction. Medical Image Analysis. 2011; 15(4):369–396. [PubMed: 21397549]
5. Merlet, S.; Caruyer, E.; Deriche, R. Parametric dictionary learning for modeling EAP and ODF in diffusion MRI. In: Ayache, N.; Delingette, H.; Golland, P.; Mori, K., editors. MICCAI 2012, Part III. LNCS. Vol. 7512. Springer; Heidelberg: 2012. p. 10-17.
6. Barmpoutis A, Vemuri B, Forder J. Fast displacement probability profile approximation from hardi using 4th-order tensors. ISBI. 2008:911–914.

NIH-PA Author Manuscript

NIH-PA Author Manuscript

NIH-PA Author Manuscript

7. Assaf Y, Freidlin R, Rohde G, Basser P. New modeling and experimental framework to characterize hindered and restricted water diffusion in brain white matter. Magnetic Resonance in Medicine. 2004; 52(5):965–978. [PubMed: 15508168]
8. Mulkern RV, Vajapeyam S, Robertson RL, Caruso PA, Rivkin MJ, Maier SE. Biexponential apparent diffusion coefficient parametrization in adult vs newborn brain. Magnetic Resonance Imaging. 2001; 19(5):659–668. [PubMed: 11672624]
9. Landman BA, Bogovic JA, Wan H, ElShahaby FEZ, Bazin PL, Prince JL. Resolution of crossing fibers with constrained compressed sensing using diffusion tensor MRI. NeuroImage. 2012; 53:2175–2186. [PubMed: 22019877]
10. Gramfort, A.; Poupon, C.; Descoteaux, M. Sparse DSI: Learning DSI structure for denoising and fast imaging. In: Ayache, N.; Delingette, H.; Golland, P.; Mori, K., editors. MICCAI 2012, Part II. LNCS. Vol. 7511. Springer; Heidelberg: 2012. p. 288-296.
11. Michailovich O, Rathi Y, Dolui S. Spatially regularized compressed sensing for high angular resolution diffusion imaging. TMI. 2011; 30(5):1100–1115.
12. Rathi, Y.; Michailovich, O.; Setsompop, K.; Bouix, S.; Shenton, ME.; Westin, C-F. Sparse multi-shell diffusion imaging. In: Fichtinger, G.; Martel, A.; Peters, T., editors. MICCAI 2011, Part II. LNCS. Vol. 6892. Springer; Heidelberg: 2011. p. 58-65.
13. Malcolm JG, Shenton ME, Rathi Y. Filtered multi-tensor tractography. IEEE Trans on Medical Imaging. 2010; 29:1664–1675.
14. Clark CA, Le Bihan D. Water diffusion compartmentation and anisotropy at high b values in the human brain. MRM. 2000; 44(6):852–859.
15. Assaf Y, Ben-Bashat D, Chapman J, Peled S, et al. High b-value q-space analyzed diffusion-weighted MRI: Application to multiple sclerosis. MRM. 2002; 47(1):115–126.
16. Behrens T, Berg H, Jbabdi S, Rushworth M, Woolrich M. Probabilistic diffusion tractography with multiple fibre orientations: what can we gain? Neuroimage. 2007; 34(1):144–155. [PubMed: 17070705]
17. Zhang H, Schneider T, Wheeler-Kingshott CA, Alexander DC. NODDI: Practical in vivo neurite orientation dispersion and density imaging of the human brain. NeuroImage. 2012
18. Jenkinson M, Smith S, et al. A global optimisation method for robust affine registration of brain images. Medical Image Analysis. 2001; 5(2):143–156. [PubMed: 11516708]
19. Rohlfing T, Zahr NM, Sullivan EV, Pfefferbaum A. The sri24 multichannel atlas of normal adult human brain structure. HBM. 2009; 31(5):798–819.
20. Kailath T. The divergence and bhattacharyya distance measures in signal selection. IEEE Tran Communication Technology. 1967; 15(1):52–60.

NIH-PA Author Manuscript

NIH-PA Author Manuscript

NIH-PA Author Manuscript

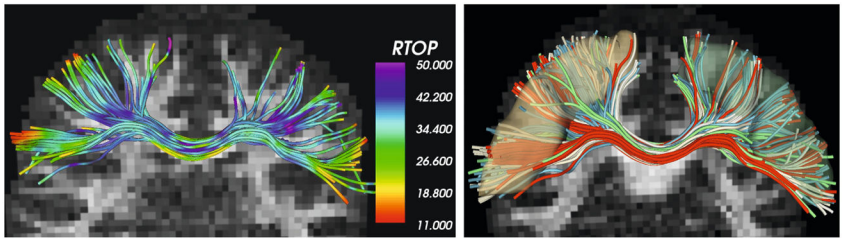

(a) RTOP (b) Tractography Comparison

Fig. 1.

(a) Tracts obtained with $N = 120$ measurements and colored using the estimated RTOP. Notice the low values (red) in the gray matter and high values (blue) in white matter, as expected. **(b)** Tracts generated using different number of measurements: red($N = 120$), green($N = 60$), blue($N = 40$) and white($N = 32$). Note the significant overlap between the fiber bundles. Overlap measure $B_{60} = 0.97$, $B_{40} = 0.94$, $B_{32} = 0.92$.

NIH-PA Author Manuscript

NIH-PA Author Manuscript

NIH-PA Author Manuscript

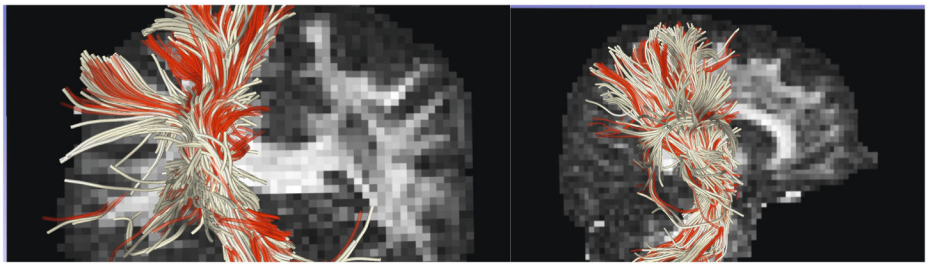

(a) Coronal (b) Sagittal

Fig. 2.

Two views of the CST. Red - fibers obtained with dense sampling ($N = 120$) and white - fibers with sparse sampling ($N = 32$). Note that, despite the sparse sampling the later method traces similar regions of the brain. Overlap measure $B_{32} = 0.9$.

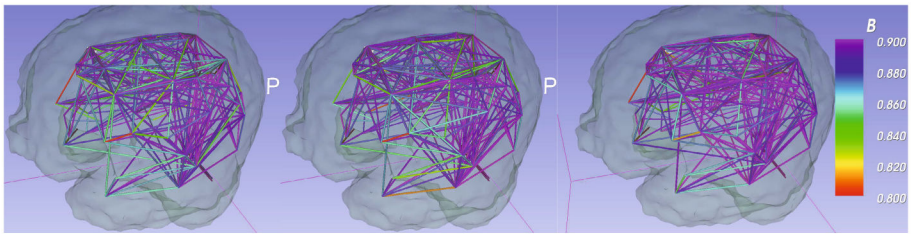

(a) N=32 (b) N=40 (c) N=60

Fig. 3.

Fiber bundle overlap measure *B* between the "gold standard" (*N* = 120) and the corresponding fiber bundles obtained from sparser acquisitions. *B* is greater than 0.8 in all cases (all acquisitions), and close to 0.9 in most cases.

NIH-PA Author Manuscript NIH-PA Author Manuscript NIH-PA Author Manuscript

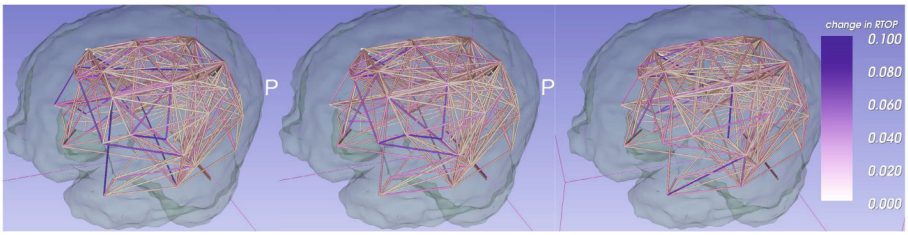

(a) N=32 (b) N=40 (c) N=60

Fig. 4.

Color coding reflects normalized mean error in estimation of RTOP compared to the “gold standard” in all fiber bundles traced for different acquisitions

NIH-PA Author Manuscript NIH-PA Author Manuscript NIH-PA Author Manuscript